Lineshape effects in photoemission from the valence states of metals

2001 J. Phys.: Condens. Matter 13 11115

(http://iopscience.iop.org/0953-8984/13/49/302)

INSTITUTE OF PHYSICS PUBLISHING JOURNAL OF PHYSICS: CONDENSED MATTER

J. Phys.: Condens. Matter **13** (2001) 11115–11132 PII: S0953-8984(01)27808-4

Lineshape effects in photoemission from the valence states of metals

T Miller and T-C Chiang

Department of Physics, University of Illinois, 1110 West Green Street, Urbana, IL 61801-3080, USA
and
Frederick Seitz Materials Research Laboratory, University of Illinois, 104 South Goodwin Avenue, Urbana, IL 61801-2902, USA

Received 13 August 2001
Published 23 November 2001
Online at stacks.iop.org/JPhysCM/13/11115

Abstract

The detailed appearance of photoelectron spectra from the valence bands of metals depends on many factors, including sample quality, and the experimental energy and angular resolution. Photoemission data are a function of at least two independent variables, the electron momentum $\boldsymbol{k}$ and the energy E; the interpretation of a spectrum can depend crucially on the mode of scanning. In addition, spectra from bulk states are influenced by intrinsic effects of the surface on the wavefunctions and the photoemission matrix element, and by the uncertainty in $\boldsymbol{k}$ caused by the finite lifetime of the excited photoelectron state. Spectra from effectively 2D systems, such as quantum wells and surface states, are free from 'final state broadening' and allow for relatively straightforward interpretations of peak widths in terms of state lifetimes. Contributions to the lifetime due to defects, phonons and the electron–electron interaction can be determined. In favourable systems and with sufficient resolution of the energy and momentum, spectra reveal non-quasi-particle behaviour of the electronic states due to many-body interactions.

1. Introduction

The study of valence electrons is central to the understanding of material properties. These electrons participate in electrical and thermal conduction, and provide the chemical bonding that governs mechanical characteristics. In a crystalline solid, valence electronic states can often be meaningfully described by band theory and a dispersion relation $E(\boldsymbol{k})$ for each band. The view of electronic structure as a set of bands occupied by independent electrons is of course an approximation. Many-body interactions complicate the situation, and one must acknowledge the possibility that the lifetime of excitations in an interacting system of particles may be so short that their energy widths become appreciable on the scale of the bandwidth, rendering the band picture useless. Perhaps typically, the reality is something in-between,

with the quasi-particle lifetime being finite but sufficiently long so that the concept is still very useful.

For over 20 years now, the premier tool for the measurement of electronic band structures of solids has been the angle-resolved photoemission spectroscopy, especially with the use of synchrotron radiation for excitation. It is often fairly straightforward to map the energy bands of a material based on the positions of peaks in photoelectron spectra, and indeed the technique has been used to map the bands of a large number of materials. In these measurements, the peak positions are the main objective; historically the widths of spectral peaks were dominated by experimental factors and so the lineshapes and widths were not of fundamental interest.

With the evolution of instrumentation and techniques of handling samples, the experimental landscape in photoemission is changing. Improvements in energy and momentum resolution have been such that it now makes sense to try to interpret peak widths as being relevant to the physical properties of the sample and the interacting system of electrons [1, 2]. A historical perspective can be found in [3], where recent results on the Ag(111) surface state are compared to earlier spectra, and are interpreted in terms of the fundamental lifetime width of this prototypical peak.

These developments have opened new avenues of research into areas such as superconductivity (not only high-T_c but also BCS-type materials [4–6]), charge-density wave materials [7, 8], the effects of scattering by impurities and phonons [9, 10] and many-body effects in general. At the same time, they demand an understanding of the different contributions to the widths and shapes of photoemission peaks from valence bands, an issue which until recently could perhaps be safely ignored in the majority of studies [11].

In any $\boldsymbol{k}$-resolved photoemission experiment, the surface plays an important role. A rough or poorly prepared surface can degrade momentum resolution or even destroy all angular information carried by the outgoing electrons. In some cases, even on perfectly prepared surfaces, a native surface reconstruction can supply numerous small $\boldsymbol{k}$ vectors for scattering and hence obscure measurements of bulk band structure. The effect of surface disorder on photoemission lineshapes from surface states, whether due to sample preparation [12] or due to some degradation that occurs during the measurement process [13], has been systematically studied. The breaking of translational symmetry at the surface also gives rise to surface photoemission, which, through a quantum-mechanical interference effect, has a significant impact on bulk photoemission lineshapes.

In a recent review, Matzdorf has discussed various experimental and physical contributions to photoemission spectral lineshapes [14]. In the current paper, some specific contributions to photoemission spectral lineshapes will be discussed. Attention is focused on dispersive electron states in metal samples, although the general ideas would be applicable to other systems as well. The effects of surface interference and final-state broadening on peaks from the bulk are presented, and the use of alternative scanning modes to the common energy distribution curve (EDC) to simplify spectra is demonstrated. Spectra from 'quantum well' samples, in which some important sources of broadening are removed, are discussed in terms of the quality of the grown films and also the photoemission process appropriate to the sample geometry. With specially prepared atomically uniform films, the linewidths can give information about fundamental scattering mechanisms involving many-body interactions, phonons and defects [15]. Finally, some high-resolution work showing non-quasi-particle behaviour due to the electron–phonon interaction will be briefly reviewed. Again in this case an alternative to the EDC, the momentum distribution curve (MDC), provides simpler lineshapes and a clearer view of the electronic structure [5].

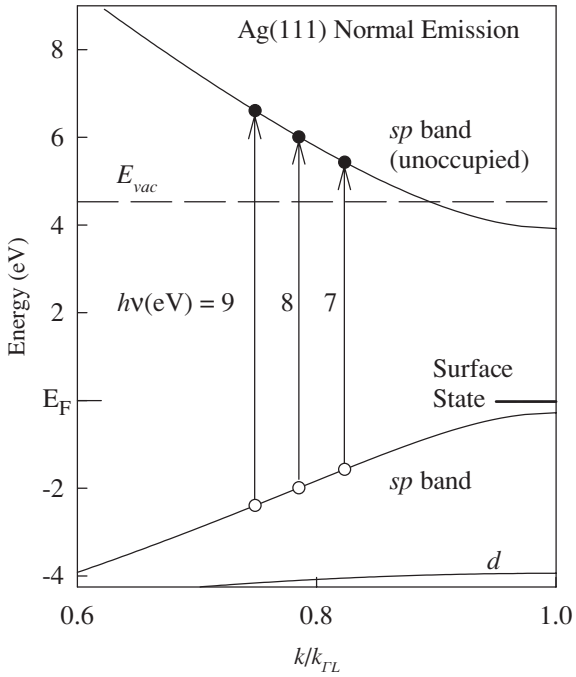

Figure 1. Band structure of Ag along the (111) direction near the *L* point. Curves show occupied sp and d bands as well as an unoccupied sp branch. Some direct transitions, for photon energies of 7, 8 and 9 eV, are shown by vertical arrows.

2. Photoemission from bulk states and surface interference

As noted in the introduction, the surface must always be considered in the interpretation of photoelectron spectra. For the study of the bulk, the traditional 'three-step' model conceptually separates bulk photoexcitation from the effects of the surface [16]. Crystal momentum is conserved in the bulk photoexcitation process, the momentum of the incident photon being generally negligible. As the excited electron exits the solid it must overcome the barrier of the work function, but its components of momentum parallel to the surface are unchanged. Because of this conservation of parallel momentum, in the 'normal emission' experimental geometry, only that part of the band structure with crystal momentum $\boldsymbol{k}$ aligned with the surface normal will be seen. Figure 1 shows the relevant part of the band structure for a photoemission measurement at normal emission from the (111) surface of Ag [17–19]. The photon energies considered here are just above the amount needed to excite electrons to states above the vacuum level so that they can escape from the solid and be detected. The conservation of crystal momentum forces the allowed photoelectric transitions to connect states of the same momentum in the reduced zone, that is, they appear as vertical transitions in a band diagram such as figure 1. Then, energy conservation allows only transitions between the occupied and the unoccupied bands that are separated by the photon energy. Three such allowed 'direct transitions' involving the dispersive sp states are shown in the figure. Also shown is the energetic position of a surface state for this system. Although, being a surface state, its component of momentum normal to the surface is ill defined, it is associated with and lies within the 'relative gap' between the occupied and the unoccupied sp bands at the *L* point [20–23].

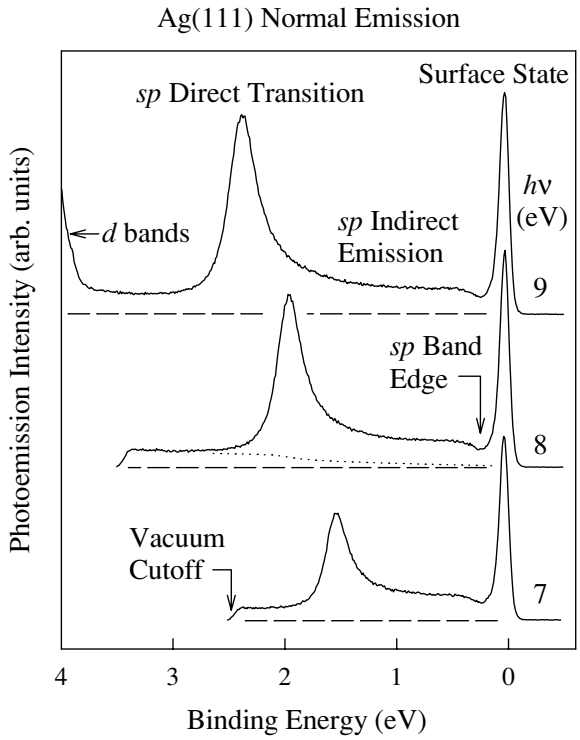

Figure 2. Normal-emission photoemission spectra from Ag(111) taken with photon energies corresponding to the direct transitions depicted in figure 1. Various spectral features are labelled. The dashed horizontal line under each curve is at the zero of intensity for that spectrum, and the dotted line is a representation of the inelastic background for the middle spectrum. The binding energy scale is relative to the Fermi level.

Figure 2 shows normal-emission photoelectron spectra taken at photon energies corresponding to the transitions shown in figure 1 [24]. These are the usual angle-resolved EDCs in which the kinetic energy setting of the analyser is swept while the photon energy and the electron emission angle with respect to the sample are kept constant. In each spectrum the surface state mentioned above can be seen as a sharp peak at a constant binding energy, near the Fermi level. It is visible through indirect transitions regardless of the photon energy [2, 3, 25, 26]. The other prominent feature is the sp direct transition peak which moves in binding energy as the photon energy is varied, in accordance with the allowed direct transitions in the bulk. By following the motion of this peak with photon energy and with knowledge of the final state band, the occupied band may be mapped out. Since it is usually possible to approximate the final state band using, for example, a free-electron-like dispersion, this technique has considerable power in determining the electronic structure of materials [27]. At a photon energy of 9 eV (top spectrum in figure 2), the energy is just high enough to allow transitions from the Ag d-bands to above the vacuum level, and this results in the peak coming in from the left-hand side of the figure.

Going beyond peak positions, these spectra are surprisingly rich in details which are difficult to reconcile with the three-step model of photoemission. First of all, the sp direct transition peaks are wide, much wider than the surface state peak in the same spectrum, for example. They are also noticeably asymmetric, with a tail extending off their right-hand

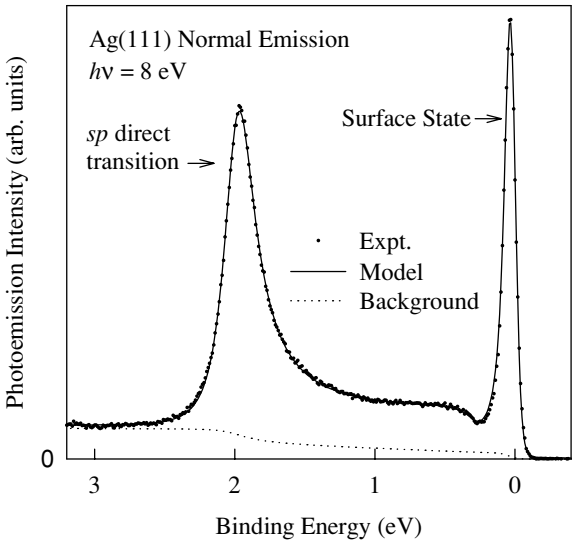

Figure 3. Model fit (solid curve) to the experimental spectrum (dots) for Ag(111) taken with a photon energy of 8 eV. The dotted curve under the spectrum is the inelastic background function. The zero intensity is at the bottom of the *y*-axis as shown.

sides. On the basis of the three-step model, one would expect to see a symmetric peak due to the direct transition. The tail melds into a fairly flat continuum (labelled 'sp indirect emission') that extends almost up to the surface state: this intensity could be ascribed loosely to electrons excited from all points on the sp band via non-vertical transitions, reflecting a 'one-dimensional density of states' along the (111) direction. However, it rolls off smoothly towards the baseline near the top of the sp band, which is the opposite of what is expected based on the density of states, which peaks sharply near the top of the band. On the high-binding-energy side of the direct transition peak, the spectrum is considerably lower. The behaviour of this 'background' is not consistent with the expected build-up of secondary electron emission towards lower kinetic energies (the dotted curve in figure 3 shows a 'Shirley background' simulating inelastic scattering).

All these features can be explained by a one-step model which integrates the effect of the surface into the photoemission process. The surface has influence in two ways: by affecting the wavefunctions in the solid near the surface where much of the spectral intensity comes from, and by contributing directly to the photoexcitation matrix element [16],

$$\left\langle \psi_{\mathrm{f}} \left| \frac{\boldsymbol{A}\cdot\nabla + \nabla\cdot\boldsymbol{A}}{2} \right| \psi_{\mathrm{i}} \right\rangle = \left\langle \psi_{\mathrm{f}} \left| \boldsymbol{A}\cdot\nabla + \frac{(\nabla\cdot\boldsymbol{A})}{2} \right| \psi_{\mathrm{i}} \right\rangle. \tag{1}$$

Here ψ_{i} and ψ_{f} are the initial- and final-state wavefunctions, respectively, and $\boldsymbol{A}$ is the vector potential of the exciting electromagnetic field. The first term on the right-hand side provides the usual direct transitions in the bulk, and includes the conservation of crystal momentum. The second term involving $\nabla\cdot\boldsymbol{A}$ is significant only near the surface and is usually ignored. On first inspection, this term might be expected to contribute only an uninteresting background to a spectrum. However, a spectrum is related to the square of the entire matrix element. This means that the bulk and surface terms are mixed in a phased sum and the possibility of quantum-mechanical interference exists. The situation is analogous to the interference between discrete and continuum excitation channels that occurs in atomic spectra, which leads to asymmetric peaks with the well-known Fano profile [28].

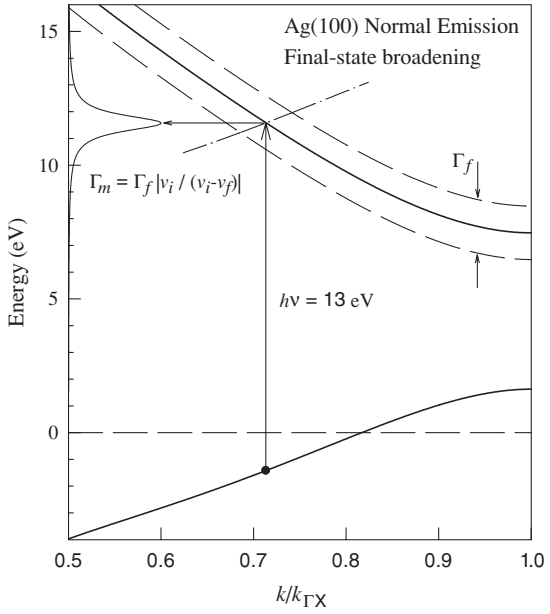

Figure 4. Schematic representation of final state broadening, using the sp bands of Ag along the (100) direction (solid curves) as an example. A constant full-width at half-maximum for the final state Γ_f is indicated by the dashed curves. For simplicity the width of the initial state is ignored. A direct transition for a photon energy of 13 eV is shown by the vertical arrow. The dash–dot curve represents a segment of the initial band translated upwards by the amount of the photon energy. The intersection of this curve with the broadened final state produces the peak seen in an EDC. The observed width of the peak Γ_m is related to Γ_f according to the formula shown, where $\boldsymbol{v}_i$, $\boldsymbol{v}_f$ are the group velocities of the initial and final bands, respectively.

The matrix element in equation (1) can be used to model photoemission spectra via Fermi's golden rule, and the result is shown in figure 3. The surface term is approximated by $C\psi_f^*(0)\psi_i(0)$, where C is a complex fitting parameter and the wavefunctions are evaluated at the surface. Two-band model wavefunctions are used inside the crystal with appropriate matching to functions on the vacuum side of the surface, which is taken as an abrupt barrier. The details can be found in [24]; here we note some features of the result. The fit of the model to the experimental data is quite good, and the value of the fitting parameter C can be related to the optical constants of the material [29]. The asymmetry of the direct transition peak stems from the interference between the bulk and the surface terms, and cannot be seen with either one alone [30]. Finally, the roll-off of the indirect transition continuum is due to the suppression of the initial-state wavefunctions near the surface as one approaches the L point in $\boldsymbol{k}$ space; this is a consequence of the surface boundary condition applied to ψ_i [31].

3. Final-state broadening and kinematic compression of linewidths

In a typical ultraviolet photoemission experiment, the mean free paths of the escaping electrons are rather short. Correspondingly, the lifetime width of the final band is substantial, $\sim$1 eV or so [32]. Of course, this large energy width is not directly manifest in the photoelectron spectrum; however, it does come into play to the extent that the final band dispersion is used to determine $\boldsymbol{k}$. The effect known as 'final state broadening' is illustrated in figure 4, using normal emission from Ag(100) as an example. A lower, partially occupied, sp band and an

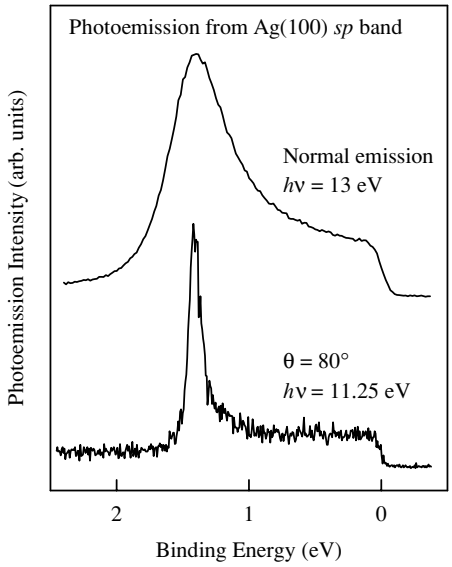

Figure 5. Normal-emission (top curve) and grazing-emission (bottom curve) photoemission spectra of a bulk direct transition in Ag. The photon energies were selected to yield a peak at about the same binding energy in the two spectra.

upper, unoccupied, sp band are shown. The vertical arrow marks the centre of a vertical transition for a photon energy of 13 eV. A constant width is assumed for the upper band (final state) and is marked by the two dashed curves above and below the central curve. One can view the photoexcitation event as lifting the initial band up by 13 eV; the matrix element is non-zero where this lifted curve intersects the broadened final state. This is shown by the dash–dot curve passing through the final band. As the kinetic energy accepted by the analyser is swept, transitions along the dash–dot curve are sampled, weighted by the lineshape of the final band. Thus a range of $\boldsymbol{k}_\perp$ values is included in the resulting peak and so it is broadened. The extra width depends on the width of the final state and the slopes or group velocities of the initial and final bands, as shown in the figure [33].

The upper spectrum in figure 5 corresponds to the situation described above. The peak is seen to be fairly broad, as is typical for many direct transition peaks seen in EDCs. In fact its width is dominated by final-state broadening. Below this is a spectrum from the same sample, with a peak from the same band at about the same energy. Despite the fact that the initial state widths would be expected to be similar for these two scans, the lower spectrum, taken at grazing exit angle instead of normal emission, displays a markedly narrower peak. This is partly because with the geometry chosen, the initial-state band happens to be flat along the direction perpendicular to the surface (group velocity $\boldsymbol{v}_{i\perp} = 0$): thus the uncertainty in $\boldsymbol{k}_\perp$ due to the width of the final state is irrelevant and the final-state broadening effect is eliminated. But also significant is the fact that the photoemission EDC at grazing emission involves not only a scan in energy but also a scan in parallel momentum at the same time. In the present case, the initial-state band is dispersing downward (yielding photoelectrons with lower kinetic energies) with increasing $\boldsymbol{k}_{||}$, while in the EDC mode, the analyser scans towards higher kinetic energy and greater $\boldsymbol{k}_{||}$ simultaneously. The result is that the EDC cuts through the direct transition faster scanning both in $\boldsymbol{k}_{||}$ and in E simultaneously than would a corresponding scan at fixed $\boldsymbol{k}_{||}$. This 'kinematic compression' effect is substantial in the

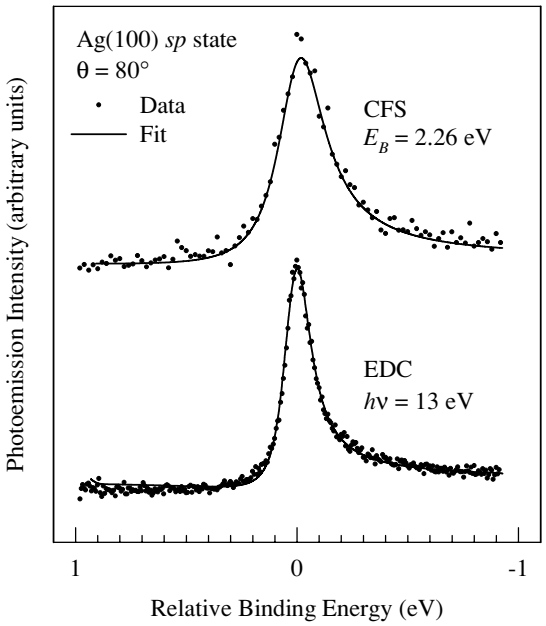

Figure 6. Comparison of photoemission spectra taken in EDC mode (lower spectrum) and in CFS mode (upper spectrum). Experimental data are shown as dots, and the curves are fits using a Fano profile. The same transition is sampled in both spectra, but in the EDC the peak is narrower due to the effect of kinematic compression.

present case, so that the observed linewidth is smaller than the inverse lifetime [34]. This can be seen by comparison to a constant final state (CFS) spectrum. In CFS spectroscopy, the photon energy is scanned while the analyser remains set at the same angle and kinetic energy. The upper curve in figure 6 is a CFS scan over the same transition as the lower EDC scan. By scanning purely in energy the true width of the peak is revealed directly in the CFS spectrum. As noted in section 3, surface–bulk interference gives rise to a Fano peak lineshape: this profile was used to fit both the spectra in the figure. From the fits, the EDC peak is narrower than the CFS peak by about a factor of 2 [35, 36].

4. Photoemission from thin films

The preceding example shows that final-state broadening is zero if the initial band is flat in the perpendicular direction, because in this case the loss of $\boldsymbol{k}$-resolution along the perpendicular direction is irrelevant. States in 2D systems, including surface states, automatically satisfy this condition, and indeed surface states usually appear sharper than bulk peaks. The problem in 3D systems is the need to resolve the perpendicular component of momentum, relying on direct transitions to a very broad final state. It was pointed out some time ago that $\boldsymbol{k}_\perp$ resolution can be obtained in another way in thin film samples [37]. If electrons are reflected off the films' boundaries and so are confined, their allowed momenta perpendicular to the film will be quantized. The situation is analogous to the one-dimensional particle-in-a-box problem in quantum mechanics. The allowed states in a well of thickness d are defined by the Bohr–Sommerfeld condition

$$2\pi n = 2k(E)d + \Phi(E) \tag{2}$$

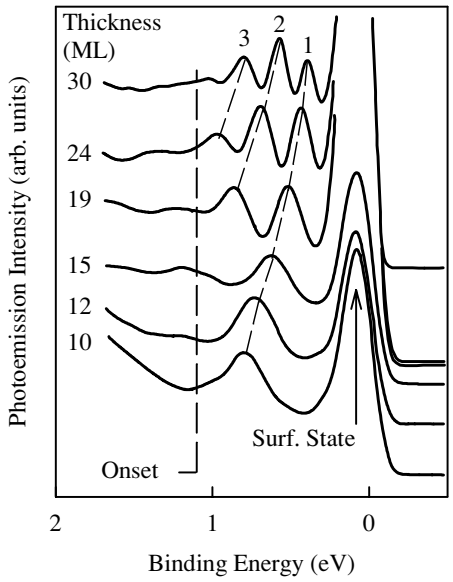

Figure 7. Normal-emission photoemission spectra using a photon energy of 10 eV for different thicknesses of Ag on Au(111) as shown. The binding energy threshold of emission is shown by the dashed line, this line is located at the top of the Au sp band along the (111) direction.

where n is an integer quantum number, $k(E)$ is the electron wavenumber as a function of the energy E and $\Phi(E)$ is the total phase shift that an electron wavefunction suffers upon reflection from both boundaries [20]. The right-hand side of equation (2) describes the phase shift of the wavefunction in completing one round trip through the film, being reflected from each boundary once. A state is allowed when this accumulated shift is an integer multiple of 2π, that is, the function describes a standing wave in the film. For a crystalline film N atomic layers thick, there will be N allowed values of k in the reduced zone. Thus, films of atomic dimensions should provide a convenient number of allowed states that would be easily resolved as separate spectral peaks.

Wachs *et al* first reported the observation by photoemission of quantized 'film states' in films of Ag supported on a Si(111) surface [38]. Subsequently it was shown that quantization occurs in Ag films on metal substrates, for example, Au, Cu and Fe, and in other systems as well [39–43]. Discrete quantum-well peaks derived from both relatively localized d-states as well as highly dispersive nearly free electron bands have been observed [44]. Ag on Au(111) is a particularly simple system because the two materials are lattice matched and have very similar electronic structures. Each material has an sp band that does not cross the Fermi level along the (111) direction. However, in Au the closest this band gets to the Fermi level along (111) is about 1.1 eV, whereas in Ag the maximum is higher, about 0.3 eV. So, in the range of binding energies between 1.1 eV and the Fermi level, sp states in the Ag film cannot propagate into the substrate and so a quantum well is formed. A set of normal-emission photoemission spectra from Ag films grown on Au(111) is shown in figure 7. The large peak on the right in each spectrum is the Ag(111) surface state. The other peaks are quantized states derived from the bulk sp band along the (111) direction. These peaks do not disperse with changing photon energy. As would be expected on the basis of the Bohr–Sommerfeld condition, these peaks crowd together as the film thickness increases. In fact using equation (2) and the positions

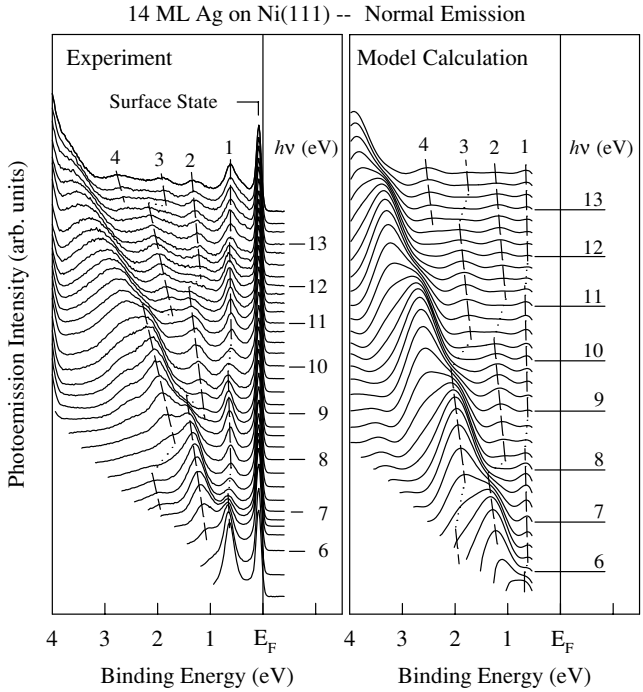

Figure 8. Experimental (left) and calculated (right) photoemission spectra for a 14 ML thick film of Ag on Ni(111) for a series of photon energies at 0.25 eV increments. Spectra with whole number photon energies are marked. The binding energy is referred to the Fermi level. The dashed lines are guides to the eye following the peak movements. The peaks are labelled with quantum numbers $n = 1$–4.

of the peaks as a function of thickness, the band dispersion may be mapped out. This is an alternative method to using direct transitions [41, 42, 45, 46].

The peaks in figure 7 are broad and not baseline-resolved. In other experiments involving building up a film by successive sub-monolayer deposits, the quantum-well peaks appear to move smoothly as more material is deposited, without showing any special behaviour at whole numbers of monolayers. This behaviour and the width of the peaks can be attributed to roughness of the film. If a film is rough on an atomic scale, the appearance of the spectra will be a function of the average thickness and will evolve continuously with coverage. Different effects may be observed depending on the scale of the roughness. An interesting example is Ag on graphite, which is not atomically flat but has large enough domains each of uniform thickness that photoelectron spectra are atomic-layer resolved. Each spectrum is the result of a superposition of contributions from different areas on the sample with different discrete thicknesses, and at least at low coverages these separate contributions can be easily seen [47]. Another Ag thin film system, Ag on Ni(111), shows quantum-well peaks that disperse with photon energy. The left panel in figure 8 shows data from one coverage of Ag on Ni(111) [48]. The peaks can be seen to undergo a complex 'ratcheting' motion as one progresses through the range of photon energies of the spectra in the figure. On the right is a stack of calculated spectra arranged to permit direct comparison with the experimental stack on the left. The calculation assumes that the electron wavefunctions scatter randomly at the substrate–film interface, thus weakening the quantization of $\boldsymbol{k}_\perp$. The main features of the model spectra then come from the evaluation of the photoexcitation matrix element over only the volume of the

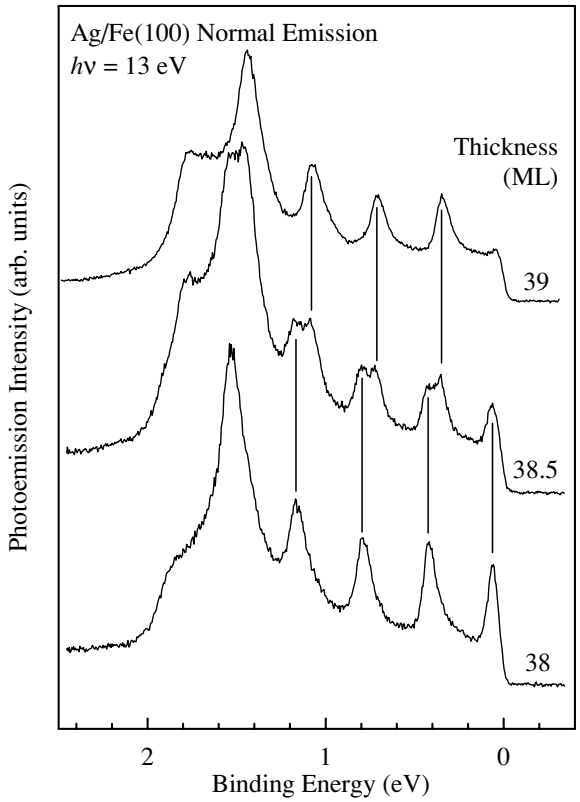

Figure 9. Normal-emission photoelectron spectra from 38, 38.5 and 39 ML films of Ag on Fe(100). The vertical lines indicate the positions of quantum-well peaks. The upper and lower scans each show one set of peaks characteristic of a single thickness, whereas the middle scan shows two sets indicating the presence of areas covered by the 38 ML and 39 ML films of Ag.

well. Again in this case the model lineshapes reflect the structural detail of the film more than they do the intrinsic electronic properties of the bulk material.

5. Photoemission from atomically uniform films

The situations described in section 4 are perhaps typical of photoemission from thin films. Quantum-well peaks are seen in a variety of systems, but the lineshapes are dominated by details of the sample configuration. An exception is found in the system Ag on Fe(100). Using a single-crystal whisker sample of Fe and a low-temperature deposition technique [49–51], films can be grown that are atomically uniform over the area of measurement. This is demonstrated in figure 9. The lowest curve in the figure is for a 38 ML thick film of Ag on Fe(100). The vertical dashed lines above this curve mark the positions of four quantum-well peaks. Unlike those in the previous examples, these peaks are sharp and baseline-resolved. Deposition of $1/2$ ML more Ag produces the middle spectrum. Following the vertical dashed lines, one can see the same four peaks that were in the bottom spectrum, plus three new peaks. Each of the new peaks is just to the right of one of the original four (it is not possible to see a peak to the right of the highest energy peak because it would be above the Fermi level), and corresponds in position with the three peaks seen in the top spectrum. The top spectrum

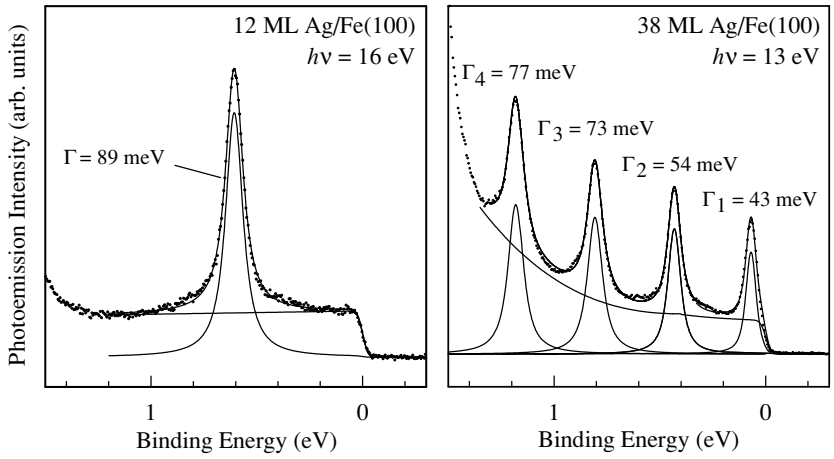

Figure 10. Normal-emission photoelectron spectra from atomically uniform films of Ag on Fe(100) with thicknesses of 12 ML (left panel) and 38 ML (right panel), using the indicated photon energies. The experimental data are plotted with dots, and the solid curves are fits to Voigt functions riding on polynomial backgrounds. The Lorentzian widths of the peaks are as indicated.

is again for a sample with an integral number of layers and again has only one set of sharp peaks. This behaviour shows that each peak is characteristic of a single film thickness in this system, and one can detect a non-integral number of atomic layers readily by inspection. This feature enables a precise calibration of the evaporator by simple layer counting [52], which in turn allows the creation of uniform films where the number of layers is exactly known up to rather large thicknesses. Carefully prepared samples of this system exhibit distinct quantum well peaks at coverages up to 119 ML [53].

With films of such perfection it is tempting to interpret the peak linewidths in terms of the inherent lifetime of quasi-particles characteristic of the bulk material. This can be done, but not by mere inspection. The difficulty can be seen by comparing spectra from different film thicknesses [54]. Figure 10 shows spectra from a 12 ML film (left panel) and a 38 ML film (right panel). The spectra have been fitted using Voigt functions for the peaks (to include the instrumental resolution and the Lorentzian widths) riding atop a polynomial background. The Lorentzian widths are marked in the figure. The four peaks in the 38 ML spectrum have widths that increase with binding energy, as might be expected on general grounds. However, the single peak in the 12 ML spectrum is wider than all the peaks in the 38 ML scan, even though it falls right in the middle of the binding energy range of the four peaks in this scan. So, there is no simple relation between the state that is sampled and its peak width; apparently the film thickness also plays a role. In fact, there is a general trend towards wider peaks for thinner films. This dependence suggests that reflection losses at the film boundaries are contributing to the peak widths because, as the film becomes thinner, an electron is reflected from the boundaries more frequently, and at each encounter with a boundary it may be lost.

An optical analogy is the Fabry–Pérot interferometer with partially reflecting mirrors and filled with an absorptive medium [55, 56]. Using this physical picture, a spectrum can be modelled with

$$I \propto \frac{1}{1+\dfrac{4f^2}{\pi^2}\sin^2\left(kNt+\dfrac{\Phi}{2}\right)}A(E)+B(E) \tag{3}$$

where $A(E)$ and $B(E)$ are smooth functions of the energy E, N is the number of layers, t is the thickness of each layer and Φ is the total phase shift upon reflection from both the substrate and the vacuum barriers. Equation (3) predicts spectral peaks in accordance with the Bohr–Sommerfeld quantization condition (equation (2)). The finesse f is equal to the ratio of peak separation and peak width. It is given by

$$f = \frac{\pi\sqrt{R}\mathrm{e}^{-Nt/2\lambda}}{1 - R\mathrm{e}^{-Nt/\lambda}} \tag{4}$$

where R is the total reflectivity of the two boundaries and λ is the mean free path in the medium. The connection to the bulk lifetime is through this mean free path. The other factors in equations (3) and (4), namely N, t, Φ and R, are properties of the thin film as an interferometer. If spectra from many different coverages are analysed simultaneously, the contributions to the peak widths from the reflection losses can be separated from those from the bulk quasi-particle lifetime. With such an analysis, the band structure and quasi-particle lifetime, as well as the phase shift and interface reflectivity can be obtained [53].

6. Sources of the quasi-particle lifetime width

In a real solid, quasi-particle states may decay due to electron–electron interactions, interactions with the crystal lattice (phonons) or because of collisions with defects. Fermi liquid theory holds that in a free-electron metal the decay rate due to electron–electron interactions should increase as the square of the energy relative to E_F. At zero temperature and exactly at the Fermi level there would be a residual width due to defect scattering and phonon emission. The contribution due to defects is expected to be independent of temperature. On the other hand, the phonon contribution would be expected to increase with temperature. In total, the peak width can be described as

$$\Gamma(E, T) = \Gamma_0 + \Gamma_1(E, T) + 2\beta E^2$$

where Γ_0 comes from defects, $\Gamma_1(E, T)$ from phonon scattering and is a function of both the energy E and the temperature T and the term $2\beta E^2$ represents electron–electron scattering [9, 15, 57]. From a Fabry–Pérot analysis of data from many thicknesses of Ag on Fe(100) at 100 K, a value of $2\beta = 25.6$ meV eV^{-1} was obtained [53]. The remaining contributions from phonons and defects should be separable through a measurement of the temperature dependence of the peak widths.

Figure 11 shows the spectra from a 19 ML thick Ag quantum well on Fe(100) at different temperatures. The dots are data points and the curves are the result of a fit to the Fabry–Pérot model including data from a 14 ML thick film [15]. Two quantum-well peaks are seen in each spectrum. Each peak broadens and becomes less intense as the temperature increases, which is consistent with the interferometer becoming more lossy as the scattering due to phonons increases. The lifetime width due to phonon scattering can be evaluated in the Debye model as [58]

$$\Gamma_1(E, T) = 2\pi\lambda \int_0^{E_\mathrm{D}} \left(\frac{E'}{E_\mathrm{D}}\right)^2 [1 - f(E - E') + 2b(E') + f(E + E')]\,\mathrm{d}E'$$

where E_D is the Debye energy (19.4 meV for Ag), and f and b are the Fermi–Dirac and Bose–Einstein distributions, respectively. In keeping with common notation, in this context λ is the electron–phonon mass-enhancement parameter, which quantifies the strength of the electron–phonon interaction. By fitting this function to widths obtained from the Fabry–Pérot analysis of data at different temperatures, a value of 0.29 for λ was obtained. The details can

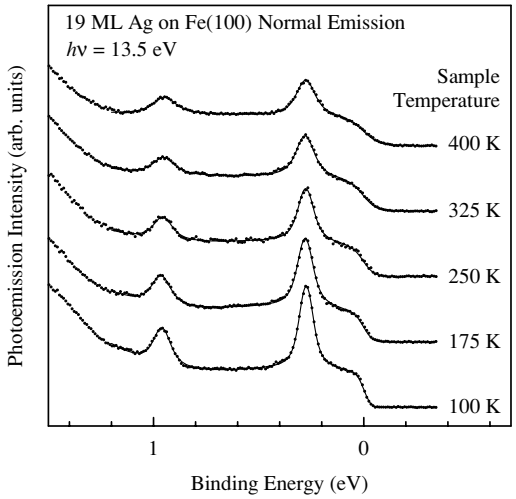

Figure 11. Spectra from a 19 ML thick Ag layer on Fe(100) at different temperatures as indicated. Experimental data are plotted with dots, and the solid curves are fits using a Fabry–Pérot model.

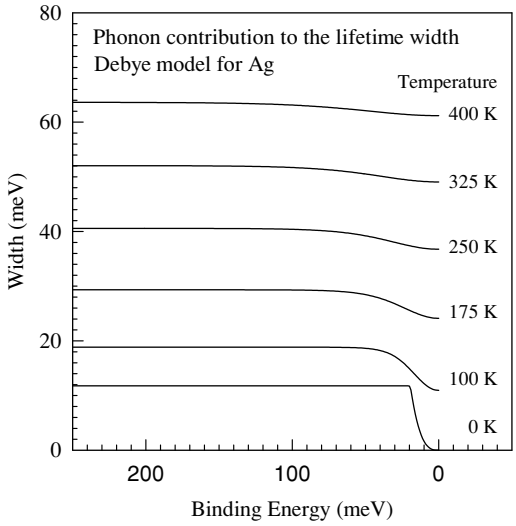

Figure 12. Phonon contribution to the lifetime width calculated in the Debye model as a function of binding energy, using the Debye energy of Ag (19.4 meV) and $\lambda = 0.29$ obtained from the analysis of the photoelectron spectra. The upper five curves are calculated for the same temperatures as the experimental data shown in figure 11 (as indicated), while the bottom curve is for zero temperature.

be found in the references; however a few results are noted here. Within 1 V or so of the Fermi level, the phonon broadening is a very significant contribution to the total width. The defect contribution is only 8 meV, corresponding to a coherence length of about 1000 Å in the absence of the other scattering mechanisms. $\Gamma_1(E, T)$ calculated using $\lambda = 0.29$ obtained from the analysis of data is shown in figure 12. There are several features of note in this model function. First, at any energy there is a significant temperature dependence over the range of temperatures conveniently available to the experiment. Second, at all temperatures, Γ_1 is practically independent of energy for excitations much beyond the Debye frequency on the

scale of k_BT. This condition is satisfied for the peaks discussed in the analysis above. Finally, as the temperature approaches zero, a singularity develops at the Debye energy, where the width rapidly drops for excitations closer to the Fermi level. This is significant because it signals a possible breakdown of the quasi-particle picture. The lifetime width is related to the imaginary part of the electron self-energy Σ which must be slowly varying in order for the quasi-particle picture to hold [10, 59]. For the present case, this is not a concern because the temperature and binding energies are sufficiently high. A demonstration of non-quasi-particle behaviour due to the electron–phonon interaction will be shown in section 7.

7. The electron–phonon interaction and nonquasiparticle behaviour

Considering an interacting system of electrons, a photoemission spectrum partly reflects the probability of generating a hole of momentum $\boldsymbol{k}$ and energy $E = \hbar\omega$ in a thermodynamic ensemble. This probability is given by the spectral weight function $A(\omega, \boldsymbol{k})$ times the appropriate Fermi distribution, where

$$A(\omega, \boldsymbol{k}) = \frac{\pi^{-1}\,|\Sigma_I(\omega, \boldsymbol{k})|}{[\hbar\omega - \varepsilon_{\boldsymbol{k}} - \Sigma_R(\omega, \boldsymbol{k})]^2 + \Sigma_I(\omega, \boldsymbol{k})^2}. \tag{5}$$

Here Σ_R and Σ_I are the real and imaginary parts of the electron self-energy and $\varepsilon_{\boldsymbol{k}}$ is the one-electron energy in a non-interacting system. Σ_R and Σ_I are not independent, but are related by a dispersion relation [59]:

$$\Sigma_R(\omega, \boldsymbol{k}) = P \int \frac{\mathrm{d}\omega'}{\pi} \frac{\Sigma_I(\omega, \boldsymbol{k})}{\omega - \omega'}. \tag{6}$$

In cases where Σ_I is a slowly varying function of ω, equation (5) approximates a Lorentzian of width $\Gamma = 2\Sigma_I$, shifted by a small amount Σ_R in energy—this is the quasi-particle regime where photoemission peaks follow a well-defined dispersion and their widths are inversely related to the lifetime. The peaks in the spectra discussed so far are of this type. On the other hand, a rapidly varying Σ_I can give rise to a non-trivial influence from Σ_R in accordance with equation (6) causing a serious distortion of the single-particle dispersion relation. The electron–phonon interaction at low temperature is a possible source of such an interesting behaviour, as can be inferred from inspection of the lowest curves in figure 12. Conversely, photoemission spectra can be analysed to yield information about the self-energy and therefore to explore different kinds of excitation modes that may exist in the many-body system [8].

LaShell *et al* [60] selected the Be(0001) surface state as a system in which non-quasi-particle behaviour due to phonon interactions may be observed [61]. They compared their data to calculated spectral functions. In this system the relevant Debye energy is conveniently large for experimental measurements. Using a surface state instead of a bulk transition offers the same advantage that a quantum-well peak does, that is, the problem of $\boldsymbol{k}_\perp$ resolution is solved without having to rely on direct transitions. In addition, in this case the surface state lies close to the Fermi level, in the area where the electron–phonon interaction is expected to have some structure, and the electron–phonon coupling is expected to be strong. Of course, this is not a bulk state, however, it has been argued that there should be a strong similarity in the scattering processes between surface and bulk states [9]. Figure 13 shows experimental data (left panel) and corresponding calculated spectral functions (right panel). The calculation combines equations (4)–(6) using as inputs a Debye energy of 65 meV and $\lambda = 0.65$, and for the dashed curves an additional 54 meV was added to Σ_I to simulate impurity scattering. These parameters were selected to give good agreement with experiment. The different spectra are EDCs taken at different angles with respect to the surface, and thus different $\boldsymbol{k}_\parallel$, which

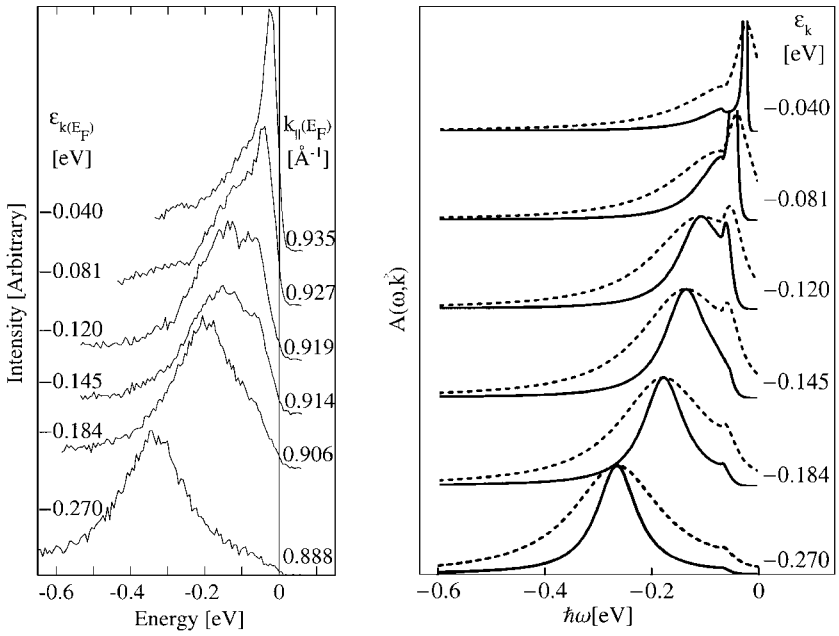

Figure 13. Left panel: photoemission EDCs from Be(0001) using the Ne resonance radiation at 16.85 eV (the contribution to the spectra from the 16.67 eV component of the radiation has been removed). Each curve corresponds to a different angle of emission from the Be(0001) surface state. The momenta (and hence $\varepsilon_{\boldsymbol{k}}$) vary slightly over each scan; the values listed apply at the Fermi level. In the lower curves a single quasi-particle peak is seen, but the spectra become more complex as the peak approaches the Fermi level. Right panel: spectral weight function calculated using the Debye model for $\omega_D = 65$ meV and $\lambda = 0.65$ (solid curves). The dashed curves include a constant 54 meV impurity scattering contribution to Σ_I and can be compared to the experimental spectra on the left. (Reproduced with permission from ref [60].)

would be the usual method of mapping the dispersion of a surface state. The resemblance between the calculated and the experimental curves is clear. In both curves two distinct features are seen: a very narrow and weakly dispersing peak that appears near the Fermi level and a relatively broad and rapidly dispersing peak at higher binding energies. Both peaks are associated with the same energy dispersion of the non-interacting state; the complex structure stems from the rapid variation in energy width with binding energy, and a substantial and rapidly varying renormalization Σ_R. In this case, the latter is strong enough to modify the non-interacting dispersion relation enough to produce the appearance of two peaks in some of the photoemission spectra.

With advances in instrumentation, such as 2D imaging spectrometers and computer-controlled analyser motions, it has become as convenient to collect spectral intensity data as a function of angle as it is to take a traditional EDC. From 2D systems, such spectra are readily converted to MDCs, and it has been pointed out that in some cases such spectra are more directly interpreted. This may be the case if the self-energy, although a strong function of the energy, is only weakly dependent on momentum. In the Debye phonon model used above, there is no momentum dependence. In this case, for a fixed energy and direction in $\boldsymbol{k}$ space, equation (5) can be written as

$$A_\omega(\boldsymbol{k}) = \frac{\pi^{-1}\Sigma_{I,\omega}}{(\hbar\omega - \varepsilon(\boldsymbol{k}) - \Sigma_{R,\omega})^2 + \Sigma_{I,\omega}^2}. \tag{7}$$

If, as over a limited range of $\boldsymbol{k}$, it is possible to regard $\varepsilon(\boldsymbol{k})$ as a linear function, this can be seen to be a Lorentzian with a width $2\Sigma_I$. Indeed, it has been shown that the data in figure 13 can be rearranged as MDCs: the result is a single peak in each spectrum which can be closely fitted to a Lorentzian lineshape [60]. Here the MDC can be viewed as an alternative mode of scanning which gives a simpler picture of the same physics.

8. Summary

Photoemission spectroscopy of metals has entered an exciting era. With improved energy and angular resolution, precise studies of electronic states are now possible. States within thermal energies of the Fermi level are particularly interesting as they contribute to many measurable material properties, such as electrical and thermal conduction. The electron–phonon interaction is an example of how an interaction with low-energy excitations (which has important physical consequences) can now be probed with photoemission spectroscopy. However, many factors influence the lineshapes and linewidths of photoemission peaks, so that even in very simple applications the spectra may have a complex appearance. For bulk states these factors include surface/bulk interference and final-state broadening. The situation is simpler with two-dimensional systems, such as quantum-well and surface states. Different modes of scanning the same area of $(E, \boldsymbol{k})$ space are available to the experimenter, which may result in spectra which are very different in appearance and in relative ease of interpretation. Despite this apparent complexity, now more than ever photoemission spectroscopy is capable of giving a most direct window into the electronic structure of metals. In particular, the nature of the quasi-particle picture and the more complex structure of the real many-body system made up of metallic valence states can be explored.

Acknowledgments

The authors thank present and former group members G E Franklin, E D Hansen, Dah-An Luh, W E McMahon, J J Paggel, and A Samsavar for their contributions to the work presented here. Much of the material presented here is based upon work supported by the US National Science Foundation under grant nos DMR-99-75470 and DMR-99-75182. An acknowledgment is made to the Donors of the Petroleum Research Fund, administered by the American Chemical Society, and to the US Department of Energy, Division of Materials Sciences (grant no DEFG02-91ER45439) for partial support of the synchrotron beamline operation and for support of the central facilities at the Frederick Seitz Materials Research Laboratory. The Synchrotron Radiation Center of the University of Wisconsin is supported by the National Science Foundation under grant no DMR-00-84402.

References

[1] Matzdorf R, Gerlach A, Theilmann F, Meister G and Goldmann A 1999 *Appl. Phys.* B **68** 393
[2] Nicolay G, Reinert F, Schmidt S, Ehm D, Steiner P and Hüfner S 2000 *Phys. Rev.* B **62** 1631
[3] Reinert F, Nicolay G, Schmidt S, Ehm D and Hüfner S 2001 *Phys. Rev.* B **63** 115 415
[4] Olson C G, Liu R, Lynch D W, List R S, Arko A J, Veal B W, Chang Y C, Jiang P Z and Paulikas A P 1990 *Phys. Rev.* B **42** 381
[5] Valla T, Fedorov A V, Johnson P D, Wells B O, Hulbert S L, Li Q, Gu G D and Koshizuka N 1999 *Science* **285** 2110
[6] Reinert F, Nicolay G, Eltner B, Ehm D, Schmidt S, Hüfner S, Probst U and Bucher E 2000 *Phys. Rev. Lett.* **85** 3930
[7] Liu R, Tonjes W C, Greanya V A, Olson C G and Frindt R F 2000 *Phys. Rev.* B **61** 5212

[8] Valla T, Fedorov A V, Johnson P D, Xue J, Smith K E and DiSalvo F J 2000 *Phys. Rev. Lett.* **85** 4759
[9] McDougall B A, Balasubramanian T and Jensen E 1995 *Phys. Rev.* B **51** 13891
[10] Valla T, Fedorov A V, Johnson P D and Hulbert S L 1999 *Phys. Rev. Lett.* **83** 2085
[11] Hüfner S, Claessen R, Reinert F, Straub Th, Strocov V N and Steiner P 1999 *J. Electron Spectrosc. Relat. Phenom.* **100** 191
[12] Theilmann F, Matzdorf R, Meister G and Goldmann A 1997 *Phys. Rev.* B **56** 3632
[13] Purdie D, Hengsberger M, Garnier M and Baer Y 1998 *Surf. Sci.* **407** L671
[14] Matzdorf R 1998 *Surf. Sci. Rep.* **30** 153
[15] Paggel J J, Miller T and Chiang T-C 1999 *Phys. Rev. Lett.* **83** 1415
[16] Feuerbacher B, Fitton B and Willis R F (ed) 1978 *Photoemission and the Electronic Properties of Surfaces* (New York: Wiley)
[17] Moruzzi V L, Janak J F and Williams A R 1978 *Calculated Electronic Properties of Metals* (New York: Pergamon)
[18] Papaconstantopoulos D A 1986 *Handbook of the Band Structure of Elemental Solids* (New York: Plenum)
[19] Smith N V and Mattheiss L F 1974 *Phys. Rev.* B **9** 1341
[20] Smith N V 1985 *Phys. Rev.* B **32** 3549
[21] Goodwin E T 1935 *Proc. Camb. Phil. Soc.* **35** 205
[22] Shockley W 1939 *Phys. Rev.* **56** 317
[23] Echenique P M and Pendry J B 1978 *J. Phys. C: Solid State Phys.* **11** 2065
[24] Miller T, McMahon W E and Chiang T-C 1996 *Phys. Rev. Lett.* **77** 1167
[25] Gartland P O and Slagsvold B J 1975 *Phys. Rev.* B **12** 4047
[26] Heimann P, Neddermeyer H and Roloff H F 1977 *J. Phys. C: Solid State Phys.* **10** L17
[27] Hüfner S 1995 *Photoelectron Spectroscopy* (New York: Springer)
[28] Fano U 1961 *Phys. Rev.* **124** 1866
[29] Hansen E D, Miller T and Chiang T-C 1997 *Phys. Rev.* B **55** 1871
[30] Hansen E D, Miller T and Chiang T-C 1997 *Phys. Rev. Lett.* **78** 2807
[31] Miller T, Hansen E D, McMahon W E and Chiang T-C 1997 *Surf. Sci.* **376** 32
[32] Samsavar A, Miller T and Chiang T-C 1990 *J. Phys.: Condens. Matter* **2** 1141
[33] Chiang T-C, Knapp J A, Aono M and Eastman D E 1980 *Phys. Rev.* B **21** 3513
[34] Hansen E D, Miller T and Chiang T C 1998 *Phys. Rev. Lett.* **80** 1766
[35] Smith N V, Thiry P and Petroff Y 1993 *Phys. Rev.* B **47** 15 476
[36] Smith N V 1992 *Comments Condens. Matter. Phys.* **15** 263
[37] Loly P D and Pendry J B 1983 *J. Phys. C Solid State Phys.* **16** 423
[38] Wachs A L, Shapiro A P, Hsieh T C and Chiang T C 1986 *Phys. Rev.* B **33** 1460
[39] Miller T, Samsavar A, Franklin G E and Chiang T-C 1988 *Phys. Rev. Lett.* **61** 1404
[40] Lindgren S Å and Walldén L 1987 *Phys. Rev. Lett.* **59** 3003
[41] Mueller M, Miller T and Chiang T-C 1990 *Phys. Rev.* B **41** 5214
[42] Lindgren S Å and Walldén L 1988 *Phys. Rev. Lett.* **61** 2894
[43] Miller T, Samsavar A and Chiang T-C 1994 *Phys. Rev.* B **50** 17 686
[44] Luh D-A, Paggel J J, Miller T and Chiang T-C 2000 *Phys. Rev. Lett.* **84** 3410
[45] Paggel J J, Miller T and Chiang T-C 2000 *Phys. Rev.* B **61** 1804
[46] Lindgren S Å and Walldén L 1989 *J. Phys: Condens. Matter* **1** 2151
[47] Patthey F and Schneider W-D 1994 *Phys. Rev.* B **50** 17 560
[48] McMahon W E, Miller T and Chiang T-C 1996 *Phys. Rev.* B **54** 10 800
[49] Evans D A, Alonso M, Cimino R and Horn K 1993 *Phys. Rev. Lett.* **70** 3483
[50] Neuhold G and Horn K 1997 *Phys. Rev. Lett.* **78** 1327
[51] Smith A R, Chao K-J, Niu Q and Shih C K 1996 *Science* **273** 226
[52] Paggel J J, Miller T, Luh D-A and Chiang T-C 2000 *Appl. Surf. Sci.* **162-163** 78
[53] Paggel J J, Miller T and Chiang T-C 1999 *Science* **283** 1709
[54] Paggel J J, Miller T and Chiang T-C 1998 *Phys. Rev. Lett.* **81** 5632
[55] Fabry C and Pérot A 1899 *Ann. Chim. Phys.* **16** 115
[56] Born M and Wolf E 1980 *Principles of Optics* 6th edn. (New York: Pergamon)
[57] Pines D and Nozières P 1966 *The Theory of Quantum Liquids* (New York: Benjamin)
[58] Grimvall G 1981 *The Electron–Phonon Interaction in Metals* (New York: North-Holland)
[59] Kadanoff L P and Baym G 1962 *Quantum Statistical Mechanics* (Reading, MA: Benjamin)
[60] LaShell S, Jensen E and Balasubramanian T 2000 *Phys. Rev.* B **61** 2371
[61] Hengsberger M, Purdie D, Segovia P, Garnier M and Baer Y 1999 *Phys. Rev. Lett.* **83** 592